



This is a repository copy of *Experiments on contaminant transport from sewer infrastructure within shallow floodwater*.

White Rose Research Online URL for this paper:

<https://eprints.whiterose.ac.uk/id/eprint/232117/>

Version: Published Version

Article:

Shucksmith, J. orcid.org/0000-0001-5497-0051, Addison-Atkinson, W., Fagour, C. et al. (6 more authors) (2025) Experiments on contaminant transport from sewer infrastructure within shallow floodwater. *Journal of Hydraulic Research*, 63 (5). pp. 521-535. ISSN: 0022-1686

<https://doi.org/10.1080/00221686.2025.2541372>

Reuse

This article is distributed under the terms of the Creative Commons Attribution (CC BY) licence. This licence allows you to distribute, remix, tweak, and build upon the work, even commercially, as long as you credit the authors for the original work. More information and the full terms of the licence here:

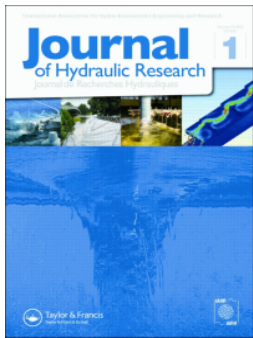
<https://creativecommons.org/licenses/>

Takedown

If you consider content in White Rose Research Online to be in breach of UK law, please notify us by emailing eprints@whiterose.ac.uk including the URL of the record and the reason for the withdrawal request.



eprints@whiterose.ac.uk
<https://eprints.whiterose.ac.uk/>



Experiments on contaminant transport from sewer infrastructure within shallow floodwater

James Shucksmith, William Addison-Atkinson, Clement Fagour, Louis Gostiaux, Nathalie Grosjean, Andy Nichols, Emmanuel Mignot, Fabio Muraro & Matteo Rubinato

To cite this article: James Shucksmith, William Addison-Atkinson, Clement Fagour, Louis Gostiaux, Nathalie Grosjean, Andy Nichols, Emmanuel Mignot, Fabio Muraro & Matteo Rubinato (2025) Experiments on contaminant transport from sewer infrastructure within shallow floodwater, Journal of Hydraulic Research, 63:5, 521-535, DOI: [10.1080/00221686.2025.2541372](https://doi.org/10.1080/00221686.2025.2541372)

To link to this article: <https://doi.org/10.1080/00221686.2025.2541372>



© 2025 The Author(s). Published by Informa UK Limited, trading as Taylor & Francis Group.



Published online: 05 Sep 2025.



Submit your article to this journal [↗](#)



Article views: 357




View related articles [↗](#)



View Crossmark data [↗](#)

Experiments on contaminant transport from sewer infrastructure within shallow floodwater

James Shucksmith^{a,b}, William Addison-Atkinson^b, Clement Fagour^{c,d}, Louis Gostiaux^c, Nathalie Grosjean^c, Andy Nichols^a, Emmanuel Mignot^c, Fabio Muraro ^a and Matteo Rubinato^e

^aSheffield Water Centre, University of Sheffield, Sheffield, UK; ^bCentre for Water Systems, University of Exeter, Exeter, UK; ^cLMFA, CNRS, Ecole Centrale Lyon, Université Claude Bernard Lyon 1, INSA Lyon, Lyon, France; ^dRiverly, INRAE Lyon, Villeurbanne, France; ^eDepartment of Civil Engineering, College of Engineering and Physical Sciences, Aston University, Birmingham, UK

ABSTRACT

Understanding the transport of soluble contamination in urban floodwater is an important aspect of public health risk assessment. However due to significant measurement complexity, there is a current lack of datasets to elucidate the associated relevant flow pathways, local velocity fields and turbulent diffusion processes. This paper evaluates three alternate experimental methodologies to quantify 2D contaminant transport at scales typical of shallow urban floodwater. It further provides a new open access dataset describing transport processes from an experimental scale model of floodwater under sewer surcharge conditions, featuring different geometrical and hydraulic configurations. Results show broad agreement between the different experimental techniques, with small but notable differences associated with measurement and experimental limitations. Results and datasets also demonstrate the considerable influence of hydraulic and geometrical complexity on transport processes, and sensitivity of the concentration levels in model street networks to heterogeneous flow pathways and velocity gradients.

ARTICLE HISTORY

Received 22 January 2025
Accepted 25 July 2025
Open for discussion

KEYWORDS

Contaminant transport processes; experimental methods; physical modelling; surface water flooding; validation dataset

1. Introduction

The removal and modification of permeable surfaces caused by rapid urbanization in many parts of the world has increased the volume of storm water entering drainage and sewer networks during rainfall events. Further, with changing global climates, some regions face prolonged and intensive rainfall at unprecedented scales (Daksiya et al., 2021). Incidents of localized sewer and urban surface water flooding are therefore becoming more commonplace in many regions (National Infrastructure Commission, 2022). During such events, drainage systems are susceptible to surcharge, which leads to interactions between overland flow and sewer networks. Surcharging sewers are hazardous, not only due to the increased water levels and velocities, but also because of the harmful contaminants carried by sewer flows (Jimoh & Abolfathi, 2022). Sewer sediments have been known to contain toxic hydrocarbons, along with carcinogenic and mutagenic heavy metals (Chen et al., 2022). Other harmful contaminants include suspended and/or dissolved material and solids, nutrients and organic matter including phosphorus and nitrogen, toxic contaminants and disease-causing micro-organisms and pathogens (Addison-Atkinson et al., 2022). Due to the complexity of mobilization, transport and transformation processes of these diverse

contaminants, a comprehensive understanding of the health risks of urban flood events is currently lacking. Small scale urban floods caused by localized high intensity rainfall events may occur relatively frequently in future (de Almeida et al., 2018; National Infrastructure Commission, 2022), hence there is an ongoing need to understand contaminant transport processes under which floodwater remains relatively shallow and is relatively likely to come into contact with local residents. Whilst the study of pollutant transport is also relevant in other context featuring low flow depths (i.e. sheet flow on hillslopes, Dahlke et al., 2012), this study focuses on urban flood contexts in which the source of contamination is a surcharging drainage network.

Dual drainage flood models are commonly used numerical tools to evaluate the risk of flooding in urban areas based on topographic models and asset information (Pender, 2006). Modelling tools are also available which consider the transport of soluble and particulate materials within sewer/drainage networks (e.g. Mannina & Viviani, 2010), although the predictive uncertainty of these approaches is often significant (Tscheikner-Gratl et al., 2019). Within surface flood flows, current challenges include the accurate determination of surface flow pathways at low flow depths, which can be significantly influenced by micro-urban

features, such as roads, kerbs, parked vehicles and the condition and design of drainage inlets (Abily et al., 2016; de Almeida et al., 2018). Gathering appropriate spatial–temporal resolution datasets of flood depths and flow velocities for model calibration and validation is therefore important to improve confidence in model predictions (Teng et al., 2017). More recently, modelling tools have been further developed to describe the transport of potential contaminants within flood water for health risk assessment (Mark et al., 2018; Sämman et al., 2019). However, contaminant concentrations within floodwater are sensitive to a number of additional processes such as turbulent diffusion, velocity shear and contaminant transformation dynamics. Furthermore, datasets describing these processes at scales appropriate to shallow urban floodwater are scarce (Mignot et al., 2023). Whilst the science of transport processes in open-channel flows is well established (Rutherford, 1994), characteristic depths (and turbulent length scales), velocity profiles, and contaminant source characteristics (e.g. surcharging drainage systems vs river banks discharges) are expected to differ considerably in shallow, highly heterogeneous urban flood conditions. In particular very few studies have considered the effects of typical street geometries, although the presence of obstructions and variations in flow pathways on contaminant transport in a fully inundated flooded street has recently been experimentally quantified (Fagour et al., 2024).

The use of experimental facilities and water laboratories to collect high resolution datasets is common to gain understanding of physical processes and to validate and compare modelling techniques (Ghoshine et al., 2009; Martins et al., 2017; Mignot et al., 2008; Moodi et al., 2024). For practical reasons, laboratory studies commonly utilize inert tracers to study the transport of contaminants in urban drainage networks and hydraulic structures (e.g. Fagour et al., 2024; Guymer et al., 2005), with techniques such as punctual conductimetry or laser induced fluorescence (LIF) available to characterize 3D mixing processes at these scales. Some studies (Beg et al., 2020; Jimoh & Abolfathi, 2022) have also focused on the transport of soluble contaminants through interaction nodes such as manholes during flood conditions, and interactions with surface flows. Beg et al. (2020) validated a CFD model describing the pipe/surface contaminant flux within a surcharging manhole utilizing measurements from a physical scale model. Rubinato et al. (2022) qualitatively considered the effects of contaminant dispersion from a flooded manhole linked to several street configurations based on the advection and mixing of a visible dye. Fagour et al. (2024) injected contaminants at different locations of a highly simplified, fully inundated, scaled flooded street network and measured the spatial distribution of scalar fluxes throughout the streets. The results from these authors highlight the

significance of urban geometrical configurations on dispersion processes. However, quantitative characterization of transport within conditions approximated to shallow surface flood water is highly challenging due to the complex 2D flow field, characteristic low flow depths, as well as the relatively large experimental scales required (Mignot et al., 2023). In such cases, point measurements of solute concentrations using intrusive probes (based on measuring conductivity or fluorescence) are often impractical when aiming to characterize the contaminant variability (temporally and spatially), as discussed by Riviere et al. (2024). Optical techniques utilizing cameras and coloured/fluorescent tracer are potentially capable of providing instantaneous characterization of 2D contaminant concentrations which are appropriate for shallow urban floodwater and drainage exceedance events. However, they normally require carefully controlled illumination which is difficult to achieve for large experimental areas, and processing and quality control of these techniques is also often challenging (Arques et al., 2018; Carmer et al., 2009). Thermal cameras have been used in some applications to quantify 2D transport (utilizing hot water as a tracer) but this methodology is limited by the need to maintain a minimum temperature difference between the tracer injection and the background flow, which may generate additional flow complexities due to convection effects. In this case the tracer is also non-conservative due to heat dissipation (Andrews et al., 2011; Cardenas et al., 2011). There is therefore a requirement to both better understand contaminant transport processes in flows of high flow width to depth ratios typical of shallow flood conditions, and further to develop and test practical but robust experimental methodologies to quantify transport processes in systems with varying geometrical and hydraulic characteristics.

In this study, we aim to utilize a scale model laboratory facility to experimentally investigate the transport dynamics of soluble contaminants emanating from a surcharging manhole within shallow urban flood conditions at realistic street scale ratios, examining the influence of varying surface geometries and hydraulic conditions on contaminant dispersion. We consider and evaluate three currently available alternate measurement techniques (intrusive pointwise measurement using conductivity probes, 2D surface thermal measurement using hot water as a tracer, and 2D colorimetry using visible dye as a tracer) aimed at characterizing the spatial and temporal spread of solutes in laboratory conditions. Furthermore, we contribute to research by generating an openly accessible dataset derived from our experimental observations, facilitating the development and validation of numerical models aimed at enhancing our understanding of contaminant transport in urban floodwater.

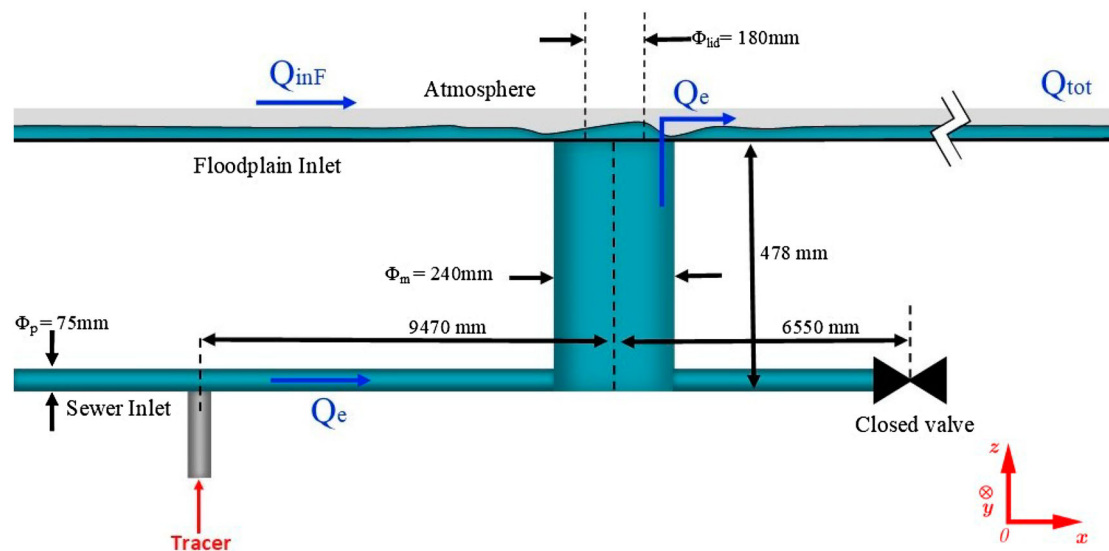


Figure 1. Experimental setup (side view).

2. Methodology

2.1. Experimental setup

All physical experiments were conducted at the University of Sheffield utilizing an experimental facility designed to consider the interaction of piped sewer and shallow surface flows via a 1:6 geometrically scaled manhole (Rubinato et al., 2017). The surface has a full width of 4000 mm, overall length of 8000 mm and slope of 1:1000. The sewer network (no slope) is characterized by 75 mm inner diameter pipework. The sewer pipe system is linked to the surface via a single vertical in-line circular manhole of 240 mm inner diameter, with a reduced fixed circular top opening of 180 mm diameter. Total inflows to the surface and sewer systems are controlled independently via upstream automated valves and quantified using electro-magnetic (MAG) flow meters. The flow enters the surface model via an inlet tank spilling over a full surface width sharp crested weir (Figure 1). For the tests described here the pipe downstream of the manhole was fully blocked such that the full sewer inflow was directed to the surface via the manhole (Q_e). This generated a steady sewer surcharge condition in all test cases, with significant localized hydraulic complexity in the vicinity of the manhole (e.g. see Martins et al., 2017).

For the work described here, the urban surface was modified to represent different potential geometrical configurations of obstructions of urban streets or avenues within high width to depth aspect ratio flows (ranging from approximately 50:1 to 120:1). Whilst these configurations are not specifically representative of the full complexity of urban topography that may be found in street networks, they were designed to recreate shallow urban flood/exceedance conditions and approximate characteristic ratios within street networks and to explore the hydraulic complexities

introduced by the common occurrence of obstructions and heterogeneous flow pathways. This was achieved by the use of premade rectangular barriers (of height > water depth) that could be rapidly installed and reoriented in various locations on the surface by use of a vacuum system to prevent any block displacement (Rubinato et al., 2022). The layout of the three configurations (termed Q, O and M series) used in this work is presented in Figure 2. In all layout cases, side barriers were used to narrow the effective flow width of the street/surface from 4000 mm to 1200 mm.

To monitor hydrostatic pressure within the experimental facility, pressure transducers (Gems series 5000, Plainville, Connecticut, USA) were installed within the bed of the surface model. These measurements were used to quantify the flow depth on the surface at various positions (S_1 – S_9). The locations of all surface pressure transducers relative to the manhole centre are presented in Table 1. Flow and depth data presented in this work represent a temporal mean of at least 180 s of data, collected in steady flow conditions after the flow had fully stabilized (after ~ 5 min for the Q series and 15 min for the other geometries). Further details of calibration procedures for flow meters and pressure sensors can be found in Rubinato (2015).

2.2. Surface velocity

A LSPIV (large-scale particle image velocimetry) system based on the use of two GoPro (San Mateo, California, USA) Hero5 Black cameras was used to evaluate the 2D free-surface velocity field within the model street. This system has previously been developed to consider velocity fields around manhole structures in drainage conditions (Arques et al., 2018; Martins et al., 2018). The first camera was positioned directly above the manhole (centred at $x, y = 0, 0$ mm), while the second was

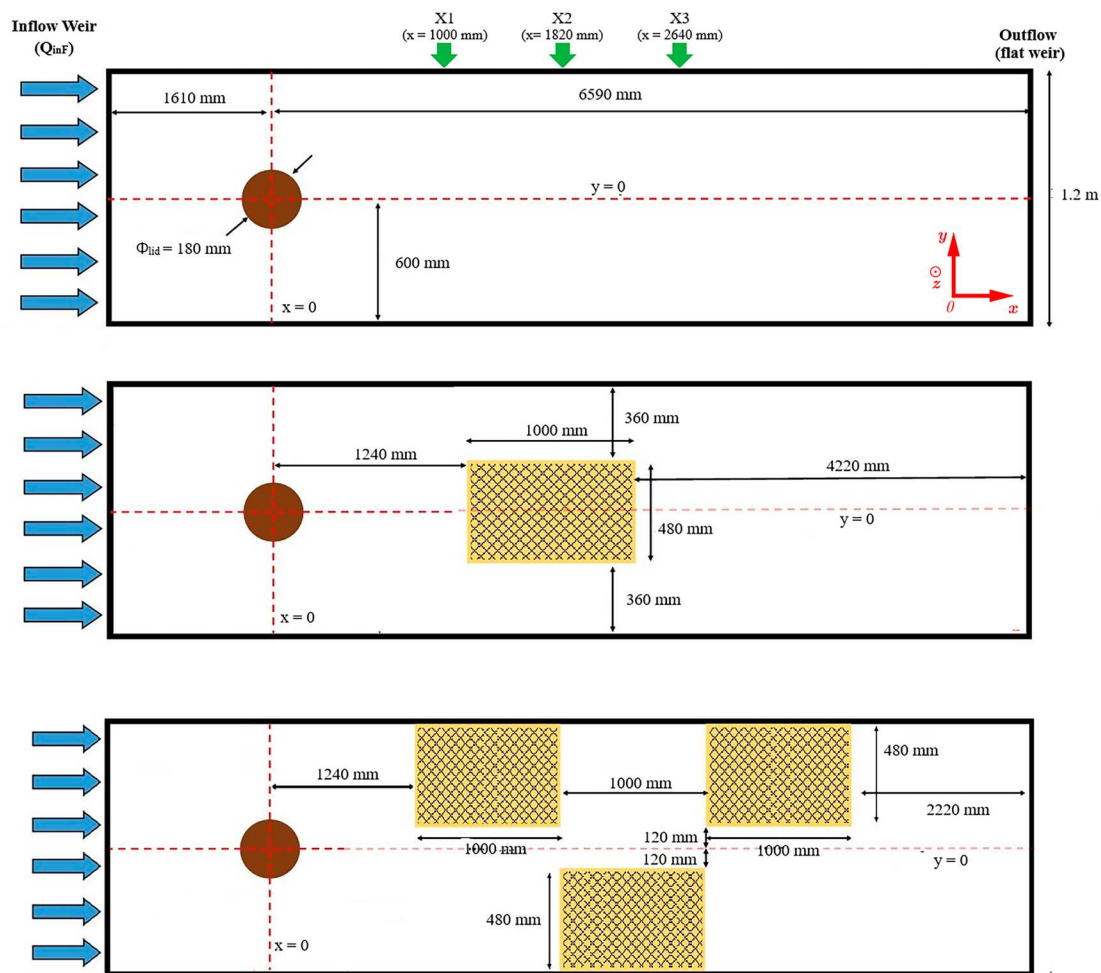


Figure 2. Three surface geometries (to view, not to scale), 1 (Top) - straight street ('Q series'), 2 (Middle) - obstacle ('O series'), 3 (Bottom) - alternate obstacles ('M series'), including positions of manhole (centre @ $x, y = 0$) and transects. Hatched and shaded areas indicate a flow obstruction.

Table 1. Position of depth measurements relative to manhole centre ($x, y = 0, 0$).

	S_1	S_2	S_3	S_4	S_5	S_6	S_7	S_8	S_9
Streamwise, x (mm)	-715	-490	-215	0	220	520	1020	3520	5610
Spanwise, y (mm)	0	0	0	-200	0	0	0	0	0

placed along the system centreline 2.3 m downstream (at $x, y = 2300, 0$ mm). Both cameras were positioned 1.65 m above the surface bed. The GoPro cameras enable selection of image and temporal resolutions; in this case a fixed image resolution of 1440×1920 pixel (along the streamwise and lateral directions, respectively), a focal length of 14 mm and an acquisition frequency of 30 Hz were used. Considering the geometry and cameras characteristics, each camera's field of view (FOV) was 3.2×4.3 m along the streamwise and lateral directions, respectively, with a spatial resolution of 2 mm/pixel. To permit the stitching of the two cameras' images to allow the spatially continuous observation of the flow field, an overlap of 0.9 m between the FOV of the two cameras was imposed. The resulting combined FOV became 5.5×4.3 m. LSPIV calibration consisted of laying out a checkerboard in the test region and collecting a short video with both

cameras. Markers were positioned in the middle of the overlapping field of view to verify the common spatial referencing of the two cameras. As the GoPro cameras contain a fisheye lens, the calibration videos were initially processed to remove the barrelling effect due to the lens. Images extracted from the videos were de-warped using a third order geometrical transformation for both cameras based on the checkerboard pattern. The images were then stitched together considering the markers positioned in the overlapping zone. The temporal alignment of the two cameras was conducted by employing a LED with a series of intermittent lights with a time resolution of 1 ms. This LED was placed in the overlapping FOV of the cameras at the beginning of each acquisition. Recordings were then aligned such that the same LED time was shown in aligned frames from both cameras. Further details of the calibration and stitching procedures can be found in Arques et al.

(2018). LSPIV tests for each experimental case were conducted by sprinkling 3 mm diameter black floating polyester particles (density = 700 kg m^{-3}) onto the flowing free surface. The LSPIV images, once spatially processed using the aforementioned procedure, were then evaluated using PIVlab (<https://www.pivlab.de/> or <https://github.com/Shrediquette/PIVlab>), an open-source particle image velocimetry (PIV) software. In this suite, an image pre-processing was performed to increase the images' contrast and highlight the buoyant tracers, and a mask applied over the position of the geometrical obstructions. PIV analysis was performed on these images. The resulting quantified free-surface velocity field has spatial resolution of 16 mm. Spurious velocity vectors were discarded by applying a spatial median filter. Processed datasets for each test case are in the form of a time series at each position (x, y, t) . In addition to the characterization of the 2D hydrodynamics, the overall surface flow rate (Q_{inF}) during each test case was derived from the integration of the temporal mean surface flow velocity over the cross section while assuming a ratio equal to 0.86 between the mean depth-averaged velocity and the mean surface velocity (Biggs et al., 2023). Resulting values are presented in Table 2.

2.3. Methodologies for quantification of the transport of tracers

To mimic the spread of contamination from a surcharging sewer network in shallow surface flood flows, different types of tracers were used as a surrogate for soluble contaminants present in the sewer pipe flow. Tracers were introduced into the pipe system 9.47 m upstream of the manhole at a steady rate (injection location was upstream of the flow meter). As the sewer flow surcharged from the manhole and mixed with the overland flow on the surface, the 2D spatial evolution of the tracer was quantified using three different experimental methods. In all experimental cases the flow was left to fully stabilize before tracer was introduced to the pipe (see aforementioned waiting times). Previous work (Beg et al., 2020), indicated that the injection location distance upstream was sufficient to ensure well-mixed conditions in the pipe network prior to reaching the manhole structure. Due to the low surface flow depths ($< 25 \text{ mm}$) and the vertical momentum introduced by the sewer surcharge, it was also assumed that the tracer is rapidly well mixed over the flow depth. Hence the different methodologies used herein are based on the 2D characterization of depth averaged or surface measurement of tracer and its evolution in space (downstream and transversally) and time (depending on the technique used) within the surface flow.

A total of six experiments utilizing three different surface geometrical configurations were completed, with LSPIV, flow, water depth and contaminant transport data (using the colorimetry and thermal camera

Table 2. Table of testing conditions.

Config.	Name	Flow rates (l s^{-1})		Local depths (mm)											Fr	Re	Salt/conductivity	Heat/ thermal camera	Dye/camera
		Sewer surcharge (Q_e)	Surface flow (Q_{inF})	S_1	S_2	S_3	S_4	S_5	S_6	S_7	S_8	S_9	S_{10}	S_{11}					
Straight street	Q1	0.77	1.22	NA	7.4	13.4	NA	13.6	5	9.1	6.6	NA	5440	0.610					
Straight street	Q2	1.46	1.3	14.9	14.4	17.1	14.8	14.9	12.4	13.3	11.9	12.3	10310	0.479					
Straight street	Q3	2.78	1.24	20.4	18.7	20.8	17.2	16.6	14.3	16	13.9	13.4	19630	0.528					
Straight street	Q4	1.11	0.11	8.1	8.9	10.5	7.3	9.6	6.8	8.9	7.3	8.4	7840	0.387					
Obstacle	O3	1.14	0.11	9.1	9.9	11.6	8.8	11.9	9.4	12.1	NA	NA	8050	0.250					
Alternate obstacles	M3	1.09	0.11	23.9	21.4	23.2	NA	24.1	21.9	24.4	NA	NA	7700	0.084					

NA = Not available. Reynolds number (Re) calculated based on the sewer surcharge flow (with manhole opening as characteristic length). Froude number (Fr) calculated based on flow characteristics measured at S_7 (i.e. based on $Q_e + Q_{inF}$).

methods; see below). Three of these tests were also conducted using a point based conductivity approach for the characterization of contaminant transport, which was used to evaluate the relative performance of the different experimental techniques described below. Table 2 provides details of all the tests conducted and the measurement techniques used for each case.

2.3.1. Salt tracer/conductivity measurement

In a first set of experiments, a solution of high salt concentration was used as a tracer which increases the conductivity of the manhole outflow water compared to the surface inflow water. The conductivity was then measured at different discrete locations in the surface flow, using four conductivity probes (by Endress + Hauser). As the conductivity vs salt concentration relation is linear (see Fagour et al., 2022), the calibration curves relating the water conductivity to the manhole outflow concentration can be evaluated based on conductivity measurements of the surface inflow (clear water) and manhole outflow (highest concentration). Given the low flow depths, the elevation of each probe had to be adjusted to keep it immersed underneath the free surface and at a distance larger than 10 mm from the bed. The measurement campaign considered the evaluation of three transects downstream of the manhole within the surface flow at $X1 = 1000$ mm, $X2 = 1820$ mm and $X3 = 2640$ mm (Figures 2, 4). Due to the discrete nature of the measurement technique, it was not possible to capture the simultaneous spatial and temporal evolution of tracer as it emerges from the manhole. Hence all conductivity measurements were taken in fully evolved (i.e. steady) tracer conditions. To this end conductivity measurements were left to stabilize before recording at a frequency of 1 Hz and results are a temporal average over 100 s.

2.3.2. Heat tracer/thermal camera measurement

In a second set of experiments, the pipe flow was heated by adding a limited discharge of hot water (at 60°C) in the tracer inlet (Figure 1). This resulted in manhole surcharge (Q_e) temperatures between 19.2 and 19.9°C relative to the street inflow (i.e. background) temperature of 18.3°C. This limited temperature difference between both flows is considered to have a minimal effect on the relative water densities but allows the 2D characterization of the transport of the surcharging overflow when flowing in the street using a thermal camera (Xenics Gobi + 640 GigE, Leuven, Belgium). The thermal camera was located 2 m above the bed near the downstream end of the flume, looking down at the free surface towards the manhole further upstream.

For each flow configuration, the surcharging and surface flows were first established with cold water in the manhole. Then, the hot temperature inlet was suddenly added and the 2D field of surface temperature over the whole domain was registered at a frequency of

3 Hz and a spatial resolution that depends mainly on the streamwise position: due to the camera angle, the spatial resolution is higher in the downstream part than the upstream part of the street. Measurements were conducted from the moment of tracer emergence from the manhole until the temporal evolution of the thermal image became negligible (i.e. fully evolved/steady mixing regime). As for all optical 2D methods, the thermal camera measurement requires the images to be orthorectified to the Cartesian axis system presented above. This was subsequently performed by placing 40 resistors at known 2D locations and at an elevation above the bed equal to the water depth and recording the pixel location corresponding to these hot points on the images (without moving the camera).

2.3.3. Dye tracer/optical camera colorimetry measurement

The third methodology is based on the introduction of a visible dye (Rhodamine WT) as a tracer in the sewer pipe flow. The overhead camera system (as used in the LSPIV tests) was used to measure the 2D light intensity and derive relative depth averaged concentration at each 2D position. This methodology was originally presented in Arques et al. (2018) for flows in a conventional laboratory flume. Further to the de-warping and stitching procedure, a colour-based calibration was required to link image green intensities to the dye concentrations at each spatial location. Ten different uniform dye concentrations were produced in the facility at three different depths under controlled lightning. These conditions were imaged to produce a specific set of calibration curves according to the observed (fixed) water depth. A third order regression was performed on the image green intensities for the given concentrations, allowing to have a calibration curve specific for each pixel. As the colour calibration procedure was performed with still water while tests were affected by surface waves, to mitigate the presence of outliers due to the surface agitation, the spatial resolution was reduced from 2 mm to 10 mm per pixel. The resulting 10×10 mm squares consisted of the average of the green intensities over that area. For each test the calibration curves were applied to the videos to obtain the resulting instantaneous dye concentrations at each timestep. In most cases the presence of surface waves interacted with lighting hence some regions along the test area borders and at different transects were affected by flickering. A seven-frame time filter and a 50×50 mm spatial median filter were applied to these regions to reduce the influence of the lighting. Similar to the heat camera tests, the 2D images were captured from the period of ejection from the manhole, however due to the need to capture and dispose of the dyed water on exit from the flume in tank of limited capacity, in some cases (O and M series tests) the fully evolved/steady mixing conditions were not reached.

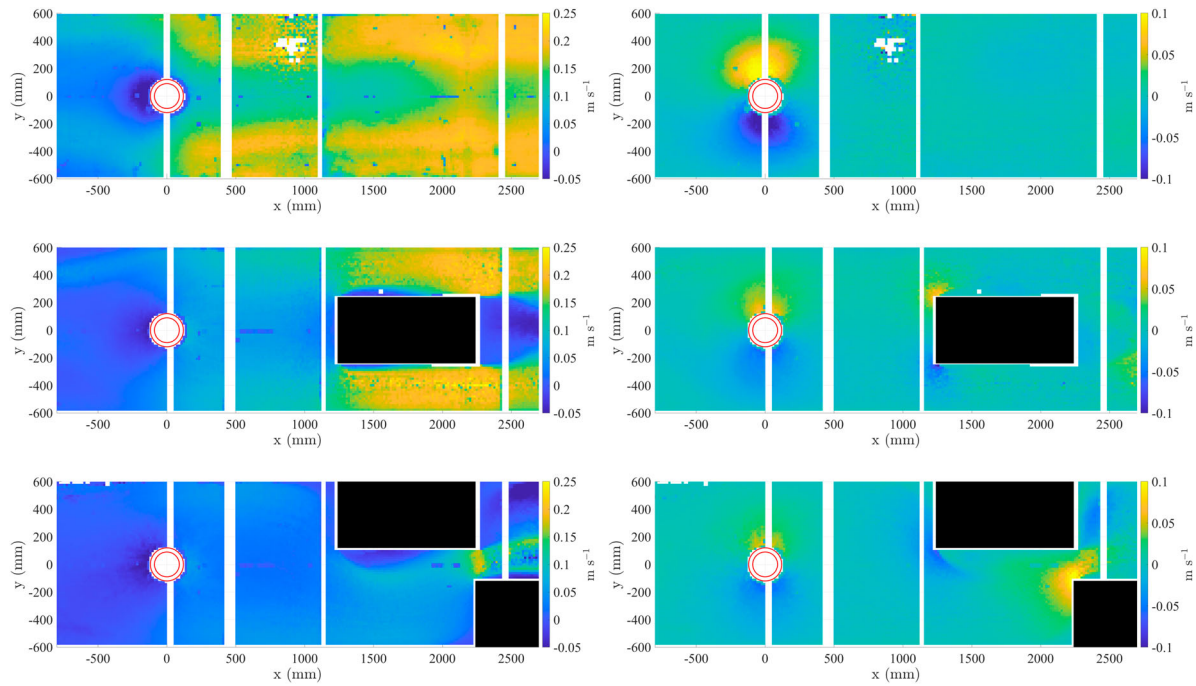


Figure 3. Streamwise (left) and spanwise (right) time-averaged surface velocity for Q3 (top), O3 (middle) and M3 (bottom) experimental cases based on LSPIV. White regions indicate areas where data is not available or removed due to filtering, red circles indicate inner and outer manhole circumference.

3. Results

Full datasets and results for all test cases are available to download at the Zenodo open access project site (see Muraro et al., 2025). In this section a limited subset of results is presented, with the aim of evaluating the relative agreement between the experimental methods and providing a general description of the hydrodynamics and contaminant transport mechanisms in shallow flood flows affected by sewer surcharge with complex street geometries. Sewer overflow transport results are presented from both evolving conditions (i.e. the tracer is emerging from the manhole through the surface flow so that temporal tracer concentration is non-stationary), and steady/fully evolved (conditions in which the temporal mean of the tracer data has become stationary at all positions).

3.1. Velocity fields and depth profiles

Example mean LSPIV 2D surface velocity data is presented in Figure 3 for each geometrical configuration case to elucidate the overall (steady-state) flow regime. Figure 4 presents velocity vector maps of the time-averaged velocity field. Figures 3 and 4 illustrate the considerable influence of the manhole surcharge. In the case of Q3 (where $Q_e > 2.5 Q_{inF}$), the manhole surcharge flow strongly displaces the surface inflow, generating strong outwards streamwise and spanwise velocities around the manhole, as the incoming surface flow is held upstream of the manhole and deflected to

the edges of the street width. Downstream of the manhole, the flow is uneven, with a bimodal distribution of streamwise velocities (i.e. with higher velocity towards the side of the channels). Hence the overall flow structure is analogous to a shear layer between the sewer efflux flow and surface inflow dominated regions. Further examination of LSPIV data from cases Q1 and Q2 show that the shear layer position is governed by the magnitude of the sewer surcharge (this is not displayed here but can be also observed in section 3.2). Further downstream, lateral velocities show a very small overall movement of mass back from the edges into the centre. As expected flow depths (Table 2) in the vicinity of the manhole (S_{1-6}) for all cases are dominated by the complexity of the local surcharge, whilst depths measured well (> 1 m) downstream of the manhole (S_{7-9}) in straight configurations show that the overall flow velocity is slightly accelerating in most cases, exhibiting a drawdown profile toward the flume end weir. Measurements of flow depth downstream of the manhole in O and M series tests are inhibited by the presence of obstructions.

As expected, flow cases featuring obstructions exhibit further hydraulic complexity around obstacles, including local accelerations through narrow sections, and recirculation zones behind obstructions. Under the M3 case, the flow exhibits higher depths overall, and the flow recirculates upstream of the manhole to a greater extent than in the cases without obstructions, with significantly lower mean velocities (however this case is also under significantly lower inflows).

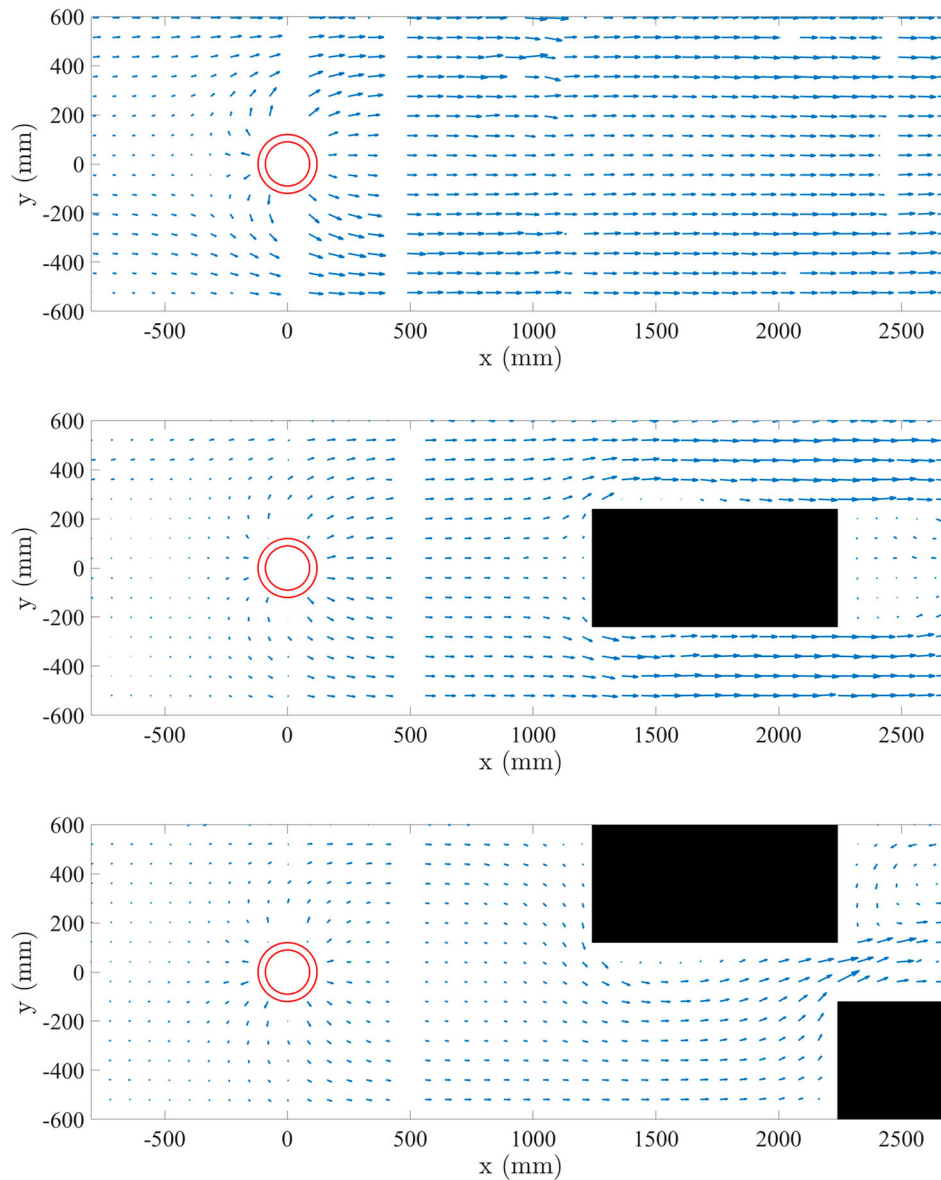


Figure 4. Vector maps of the time-averaged velocity field for Q3 (top), O3 (middle) and M3 (bottom) experimental cases based on LSPIV. To facilitate visualization, one vector every five is displayed. White regions indicate areas where data is not available or removed due to filtering, red circles indicate inner and outer manhole circumference.

3.2. Comparison of tracer measurement techniques in a straight street (steady/fully evolved tracer conditions)

Figure 5 presents direct comparison of the spatial distribution of temporally-averaged tracer concentration at three transects downstream of the manhole within fully evolved flow and tracer conditions using the three measurement techniques. Results are presented for three different hydraulic conditions, under the straight street configuration (Q series). Due to the different characteristic tracers used, normalized results are presented, with the range representing the difference between the concentration of the surface inflow (0) and the manhole surcharge (1, based on the measured concentration immediately downstream of the manhole). For the Q3 flow condition, the three techniques provide very similar transects at all the measurement locations

downstream of the manhole, with a slightly higher levels of experimental noise from the heat/thermal measurement based technique. For the lower flow rates, some variations between the techniques are observed, with the heat/thermal and salt/conductivity measurements being in generally closer agreement for the Q2 flow condition at X2 and X3, and the dye/camera based technique resulting in a slightly wider spread of solute. Results for Q1 are more mixed, with the salt/conductivity being in closer agreement to the dye/camera concentrations on one side of the plume, and closer to the heat/thermal measurement on the other side of the plume. Overall, in the Q1 condition, the dye/camera reports the highest transverse mixing of tracer, followed by the salt/conductivity, with the heat/thermal technique resulting in the lowest spread. It should be noted that due to practical limitations each of these techniques were tested independently

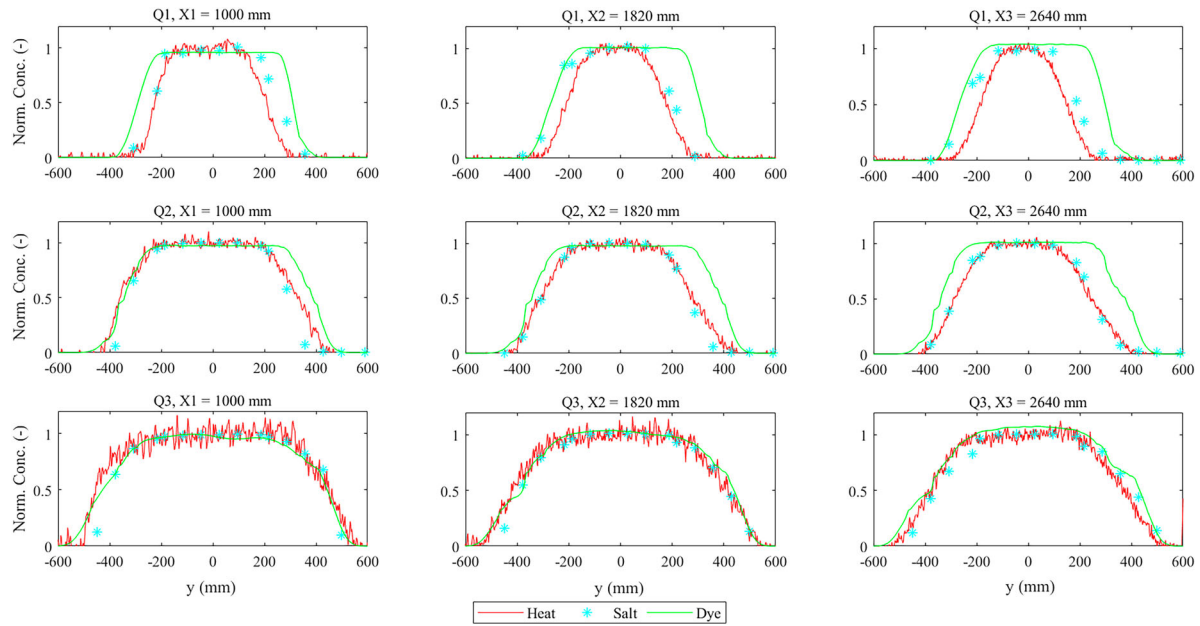


Figure 5. Comparison of measurement techniques (conductivity/thermal/colorimetry) at three transects: $X1 = 1000$ mm (left column), $X2 = 1820$ mm (centre column), $X3 = 2640$ mm (right column), relative to the manhole centre downstream of surcharging manhole for Q1 (top), Q2 (middle) and Q3 (bottom) flow configurations. Temporal average of normalized values in fully evolved/steady flow and tracer conditions.

(i.e. the flume was reset between measurements), hence given the sensitivity of mixing processes to variations in velocity fields, it is likely that some deviation is caused by small variations in experimental conditions (temperature, flow valve opening, side wall positions) between tests.

Figure 6 presents the normalized 2D spatial distribution of temporally averaged tracer measured using the thermal and colorimetry methods (which both permit visualization of the entire 2D plume) within fully evolved conditions. Results are presented for three different hydraulic conditions, under the straight street configuration (Q series). Downstream of the manhole the 2D visualizations largely concur with the analysis of the transects. The highest flow rate (Q3) exhibits the highest similarity between the two techniques, with minimal transverse mixing of the dye downstream of the influence of the manhole, and minimal concentration gradients within the central region of the plume at $x \approx > 100$ mm and -200 mm $< y < 200$ mm. For the lower flow rates (Q1 and Q2) the heat/thermal measurements suggest a slight transverse narrowing of the plume beyond approximately $x = 1500$ mm, with the reported plume width remaining approximately constant when using the dye/camera based technique. This effect may be due to net advection from the flume edges into the channel centre, downstream of the influence of the initial momentum from the manhole surcharge (see Figure 3), or a technique-specific issue such as cooling of the tracer at the plume edge. The local area in and around the manhole also appears differently under the two techniques. For the Q3 case, concentrations in the upstream vicinity of the manhole

appear high (> 1); this may also be due to local areas of high flow depth disturbance around the manhole due to the localized effect of the sewer surcharge under high Q_e values (as this method is sensitive to flow depth), or alternately localized intermittent light reflections caused by complex surface flow patterns in this area.

3.3. Temporal evolution of tracer around a central obstruction (thermal and colorimetry techniques)

Figure 7 presents normalized instantaneous 2D spatial distribution of tracer at three time points relative to the first emergence of tracer from the manhole (i.e. $t = 0$), measured using the thermal and colorimetry techniques for case O3. Considering that tracer tests are conducted independently, comparison of colorimetry and thermal techniques show a very good agreement in terms of overall spatial extent of the tracers at the three time points. Some differences are observed in terms of concentration gradients upstream of the obstruction and around the manhole as the simulation progresses. At $t = 40$ s the colorimetry technique suggests more uniform distribution of tracer within the central plume, and sharper concentration gradients at plume edges than the thermal technique. This effect may potentially be a function of local cooling effects of the thermal tracer or differences between the depth averaged (measured using the colorimetry technique) and surface concentrations (measured with the thermal camera). It is also noted that for the dye-based techniques some local regions suffer from influence of direct lighting reflections (e.g. around $y = -400$ and

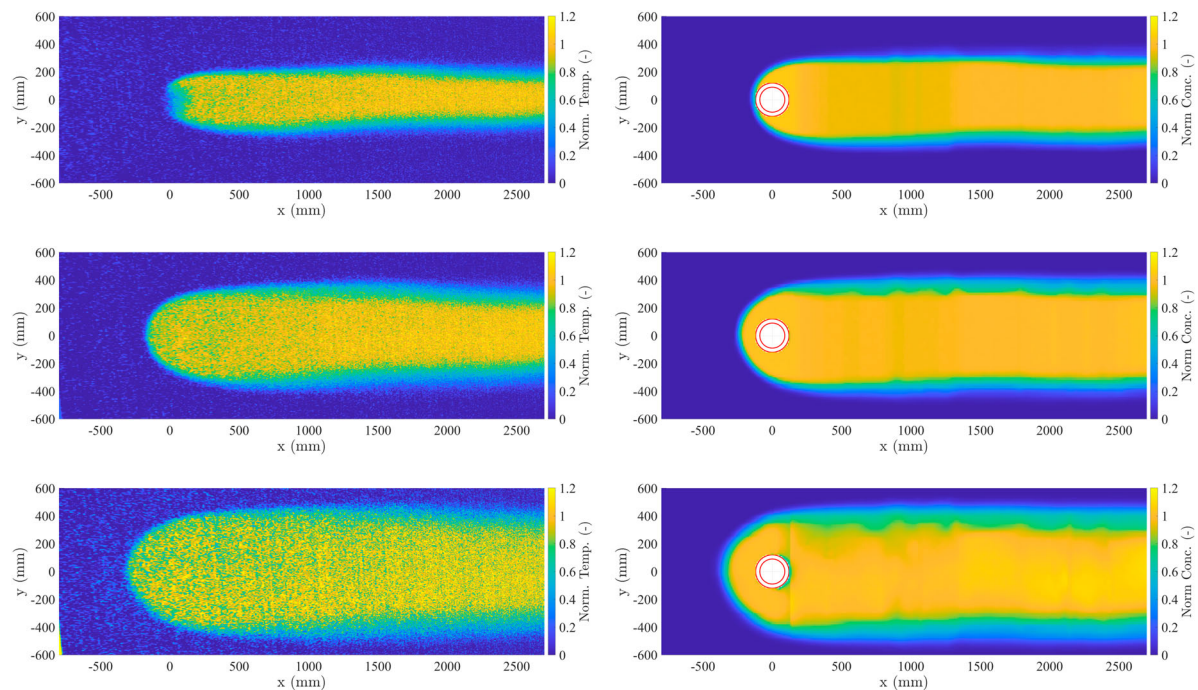


Figure 6. Normalized temporally averaged 2D spatial distribution of tracer in straight street configuration in fully evolved tracer conditions using thermal (left) and colorimetry (right) techniques over three hydraulic conditions (Q1, Q2 and Q3 on top, middle and bottom, respectively).

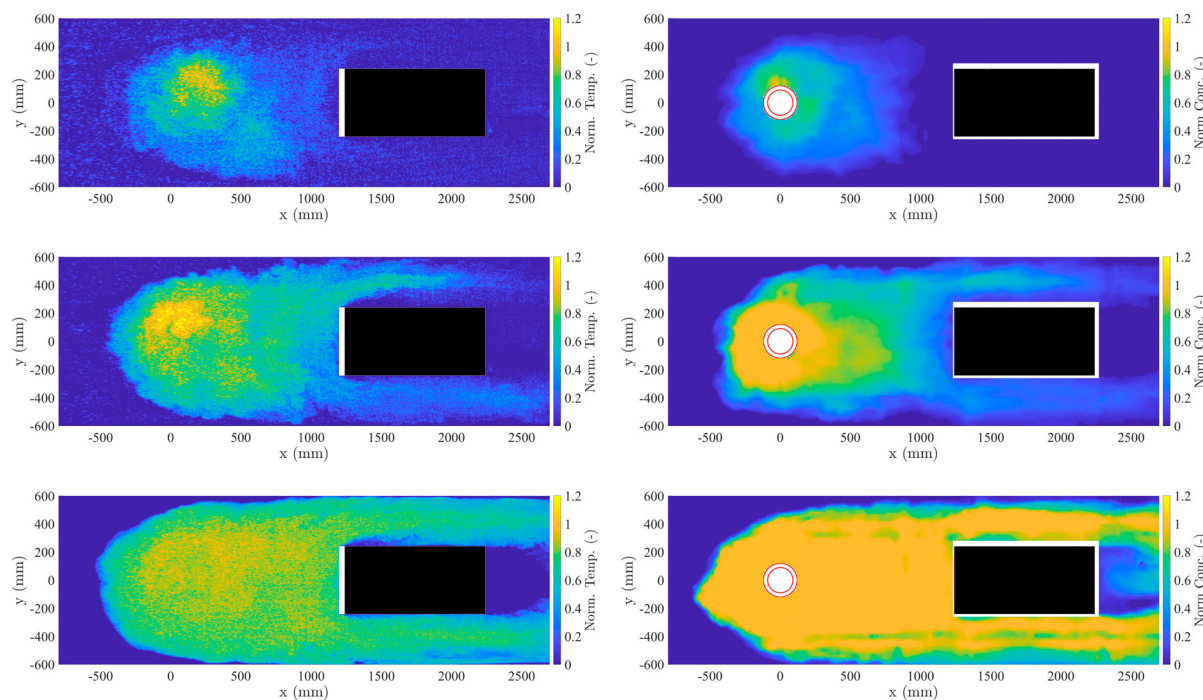


Figure 7. Instantaneous 2D spatial distribution of tracer at times relative to first tracer emergence in the presence of a central obstruction (O3 case) using thermal (left) and colorimetry (right) techniques (normalized relative to measurement at manhole out-flow). Images represent the concentration distribution after 10, 20 and 40 s (top, middle and bottom, respectively) from the initial emergence.

+400) resulting in deviations of $\sim 10\%$. Both techniques demonstrate the considerable complexity of the flow and mixing processes behind the local obstruction, in which the formation of eddy structures causes considerable heterogeneity in concentrations which persist 40 s after contaminant surcharge.

3.4. Temporal evolution of tracer through an alternate obstacle arrangement (thermal and colorimetry techniques)

Figure 8 presents normalized instantaneous 2D spatial distribution of tracer concentration at three time

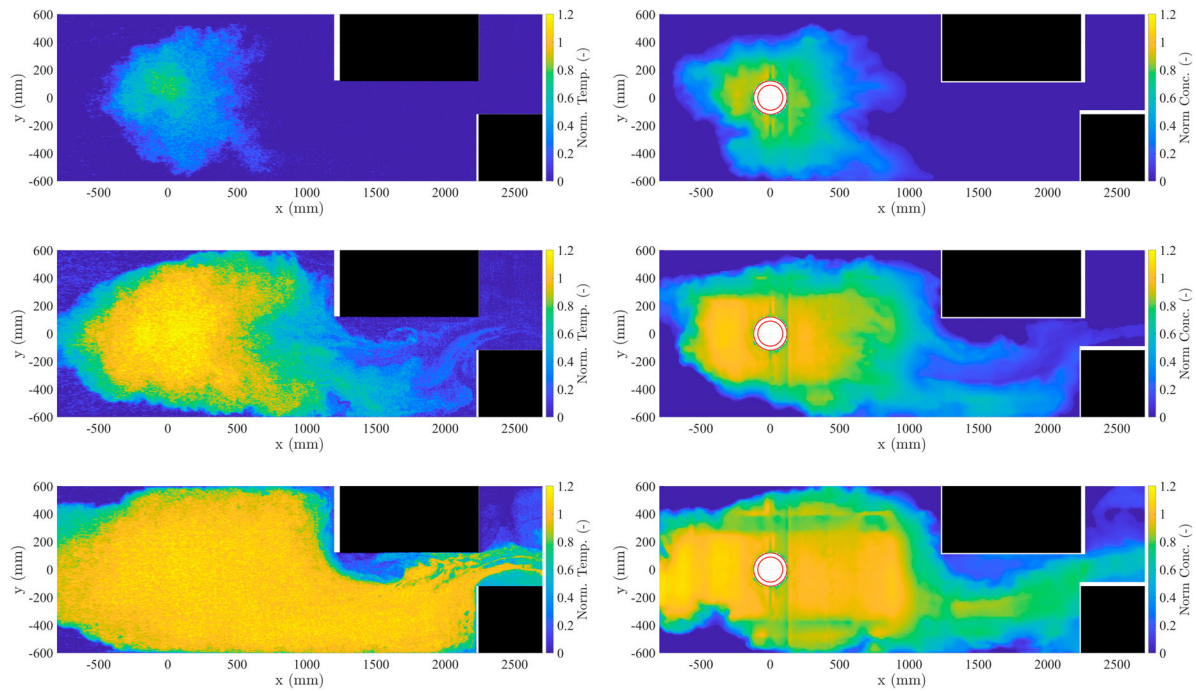


Figure 8. Instantaneous 2D spatial distribution of tracer at times relative to first tracer emergence in the presence of alternate obstacles (M3 case) using thermal (left) and colorimetry (right) techniques (normalized relative to measurement at manhole). Images represent the concentration distribution after 20, 40 and 80 s (top, middle and bottom, respectively) from the initial emergence.

points relative to the first emergence of tracer from the manhole (i.e. $t = 0$), measured using the thermal and colorimetry techniques for case M3. Similarly to the single obstacle case (O3), the temporal evolution of tracer through the alternate obstacle arrangement shows a general good agreement in terms of overall spatial extent at the three time points. Observable differences in the two techniques are associated with relative concentration magnitudes in the vicinity of the manhole upstream of the first obstruction, with the thermal technique reporting similar concentrations upstream and downstream and the dye-based technique reporting more trapping of the tracer and persistently higher concentrations upstream of the manhole potentially due to local recirculation and lower/negative velocities in this region (Figure 3). Similarly to the previous case (O3), differences may be caused by differential cooling of the thermal tracer at longer timescales due to local thermal gradients or surface vs depth averaged differences. From both Figures 7 and 8, notable features include narrow concentrated plumes within regions of accelerated flow between side walls, obstacles and recirculation zones. Around recirculation zones there is considerable heterogeneity in contaminant concentrations with low pollution zones persisting well beyond 80 s after tracer surcharge from the manhole.

4. Discussion

This paper has considered the use of three alternate laboratory measurement techniques to evaluate the spread

of tracer in flows with characteristics similar to shallow urban flood conditions, i.e. shallow depths, high aspect ratios, heterogeneous flow fields, with contaminants emerging from surcharging of an urban drainage with varying degrees of efflux and momentum. In terms of practical considerations, point measurements using conductivity probes are relatively low cost, require high levels of tracer if the number of measurement points increases, and provide robust measurements with minimal/straightforward calibration and processing requirements. Key disadvantages are associated with the nature of point measurement techniques, i.e. the impracticability of characterizing the simultaneous spatial and temporal evolution of tracer over a large measurement using a limited number of point measurements. Moreover, the measurement duration is directly proportional to the number of measurement points (including the requirement to relocate probes to different measurement positions). In contrast, the utilization of colorimetry allows an excellent understanding of the spread of soluble tracer in 2D and in temporally evolving conditions. However, limitations of this technique are associated with the need to provide controlled and constant lighting conditions. In practice this is very difficult to achieve over a large measurement area so that, in limited regions of the flow field, errors can be caused by direct light reflection on the water surface (providing a noisy optical signal). Further, due to the depth sensitivity of the technique, the calibration requirements are quite onerous (with calibration relationships required at multiple flow depths) and further errors can be considered when charactering flows with rapidly varying

depths (i.e. in this case the hydraulically complex region close to the manhole which features rapid changes in depth and velocity). For this technique relatively high concentrations of tracer are needed to provide sufficient contrast, and a high level of care must be taken over data processing and filtering. For both the conductivity and colorimetry methods, the water seeded with salt or dye cannot be reused by the experimental device (Riviere et al., 2024) and must be disposed of. Thermal measurements provide a rapid 2D view of the flow field, and as the reading is not depth sensitive, calibration is relatively easily achieved. Orthorectification of the images can be achieved using an array of well-located resistors. One major advantage is that the water can be reused, as long as the warmed water used in the experiment has time to cool down within the laboratory sump. Nevertheless, the thermal cameras remain more expensive than the optical cameras (the thermal camera used herein costs about 10,000 € vs 400 € for each optical camera), and limitations can arise in very large-scale experimental flumes and at longer timescales due to the non-conservative tracer, i.e. where thermal exchanges with the surrounding atmosphere are no-longer negligible. Furthermore, it is important to note that while the colorimetry provides a depth-averaged concentration data, the thermal camera provides 2D maps of the surface temperature. Future studies of transport processes in flows with similar characteristics should recognize that differences in 2D measurement techniques are non-trivial; however, even considering inherent limitations and associated uncertainties these methods provide valuable insights into contaminant transport processes in the challenging context of shallow floodwater and are in broad agreement regarding overall spatial extents of contaminants.

It is anticipated that datasets provided by this study will be of value to modelling groups for validation of numerical approaches for the simulation of contaminant transport processes in urban flood conditions (Mignot et al., 2023), as to the best of the authors knowledge no equivalently detailed datasets are currently available. This will enable an increased confidence in modelling of and risk assessment of waterborne public health risks during floods (Addison-Atkinson et al., 2022). Whilst overall measurement limitations should be recognized when calibrating and validating numerical models, the overall impacts of measurement uncertainty may be considered minor when considering the overall context of localized urban flood risk, whereby other modelling uncertainties (such as urban hydrology or topography) may be very significant.

The description and modelling of local flow depths around the manhole using the same physical model under similar surcharging conditions have previously been explored in Martins et al. (2017) and Moodi et al. (2024) and therefore will not be covered in further

detail here. In terms of contaminant transport process, results here demonstrate significant variation due to the complexity of the local hydraulic processes. Transport processes in free surface flows are characterized by turbulent diffusion and advection processes (Rutherford, 1994); however, in this case turbulent eddies which drive diffusion are expected to be limited by low flow depth and flow roughness conditions, and transport processes are hence largely advection dominated. This can be observed in the straight street cases, where downstream of the manhole there is very limited/negligible transverse spreading of tracer over the mixing layer, with overall plume width, transverse concentration gradients and peak concentrations largely unvarying in the region $500 \text{ mm} < x < 2700 \text{ mm}$. In these cases, it is suggested that small local advection towards the channel centreline in the transverse direction acts to counter any turbulent diffusion effects in spreading the plume.

In all cases considered here, the initial influence of the manhole surcharge and the local momentum of the flow field has a significant impact on the distribution of tracer, and hence characterization of both the mass and momentum exchange from surcharging flows is likely to be important when understanding the distribution of contaminants in urban floods with similar hydraulic characteristics. The strength of the surcharge is also significant in understanding position of the downstream interface/shear layer between the sewer efflux and surface inflows as well as the contaminant spread upstream of the manhole. In this upstream region negative streamwise velocities from the surcharge flow cause the advection of tracer against the primary direction of the surface inflow. This effect is negligible in the case of Q1, but becomes more significant as the surcharge flow is increased (Q2 and Q3).

As anticipated, the transport of contaminants is highly sensitive to the variations in local flow pathways and velocity fields, which can be significantly influenced by small or larger scale urban furniture (trees, kiosk, bus-stops, parked cars, etc.). The presence of these features forms local separation and recirculation zones, for example in the region immediately behind the obstructions in the O and M series cases, as well as adjacent to the first obstruction in the M series case (around $1300 < x < 1800$, $-120 < y < 120 \text{ mm}$). As transport is dominated by mean flow advection, strong concentration gradients persist over these regions well beyond the timescales required for complete mixing within the main flow field. The effect of downstream obstructions in providing additional flow resistance is also significant in terms of overall increased flow depths and increasing the presence of slow recirculation zones upstream of the manhole. For example, in the case of M3, the scalar velocities upstream of the manhole are very small (absolute values $< 0.05 \text{ m s}^{-1}$) over a large area (throughout the region $x < 0$). At long timescales

(≈ 140 s after surcharge) the sewer efflux and diffusion processes cause the tracer spread upstream to the measurement boundary ($x = -700$ mm) around the central flow region ($-400 < \approx y \approx < 400$), with the mean advection from the surface inflow only dominating the sewer efflux and diffusion processes towards the channel edges. Based on these results it is considered that modelling of contaminant fate in urban flood conditions is therefore likely to be highly sensitive to the faithful representation of flow fields around such urban features, requiring detailed modelling approaches and high resolution urban geometry data to achieve accurate results (Mignot et al., 2013).

It should be noted that the experimental conditions simulated in this work represent a limited subset of the range of potential flow conditions and contaminant characteristics likely to be encountered in urban flood conditions (Fagour et al., 2024). Further work may consider unsteady conditions, more complex flow structures (e.g. through street junctions) and deeper flood events with more significant vertical velocity and concentration gradients. Besides, work to date has focused on conservative neutrally buoyant tracers; however, contaminants may be positively or negatively buoyant, and can travel as sediments (Genouel et al., 2024). Finally, the longer term transport and survival/persistence of pathogens and contaminants of concern in urban soils and other surfaces require more detailed investigation.

5. Conclusions

The research presented in this study provides an examination of the transport of soluble contaminants in shallow urban floodwaters from a sewer surcharge utilizing an experimental scale model. The findings underscore the intricate interplay between hydraulic dynamics, street geometry and flow conditions which collectively govern the transport and dispersion of contaminants. By systematically evaluating three distinct measurement techniques – conductivity probes, thermal imaging and colorimetric analysis – the study highlights the relative advantages and limitations of each method in accurately capturing the 2D contaminant transport in dynamic shallow urban flooding scenarios.

Results demonstrate that contaminant transport is advection dominated and significantly affected by localized flow variations, initial surcharge/efflux momentum effects and the presence of obstructions, which alter velocity pathways and introduce complex recirculation zones. The study confirms that high-resolution data, such as that obtained from colorimetry and thermal imaging, offers a nuanced understanding of spatial and temporal solute distribution, a critical factor for model calibration in urban flood risk assessments. Although

conductivity probes offer robustness and low calibration requirements, the approach is fundamentally limited in spatial scope and ability to characterize evolving (non-steady) conditions. The 2D data from thermal and colorimetric methods is instrumental in illustrating the effects of flow obstacles, channel narrowing, and efflux momentum from sewer outflows. It should however be noted that thermal imaging is relatively costly and sensitive to environmental thermal exchanges, colorimetry requires controlled lighting and significant calibration effort, and can be susceptible to localized errors due to lighting reflections. It has been shown here that although in broad agreement, differences between experimental techniques are non-negligible in terms of characterizing specific local concentrations. These findings emphasize the importance of choosing measurement techniques tailored to specific hydrodynamic conditions and contaminant characteristics in urban flood flows, and the awareness or measurement limitations.

This research contributes a novel open-access dataset (Muraro et al., 2025) that enables the validation of operational numerical models, enhancing predictive capabilities and facilitating the accurate assessment of public health risks associated with waterborne contaminants in flood-prone urban areas. Future studies could build on this work by exploring the influence of varied contaminant densities, multi-directional flow structures, and complex urban features such as street intersections, flow intrusion into built-up or widely open areas. Additionally, investigating non-conservative tracers could further inform the modelling of contaminant persistence and biohazard distribution.

Acknowledgements

This work was funded by Co-UD labs (<https://co-udlabs.eu/>) and has received funding from the European Union's Horizon 2020 research and innovation programme under grant agreement No 101008626. The authors would also like to thank Christopher Green for technical laboratory support and Katherine Parkinson for her assistance in drafting technical figures.

Disclosure statement

No potential conflict of interest was reported by the author(s).

Funding

This work was supported by H2020 Research Infrastructures [grant number 101008626].

Notation

Fr	Froude number (of combined surface flow) (–)
Q _e	flow in sewer pipe, exchanged to surface flow via manhole (surcharge/efflux flow). (l s ^{–1})

Q_{inF}	surface inflow, upstream of manhole ($l\ s^{-1}$)
Q_{tot}	total flow (surface and sewer flow) ($l\ s^{-1}$)
Re	Reynolds number (of surcharge flow) (–)
S_{1-9}	local flow depth at measurement position S (mm)
t	time (s)
x, y	Cartesian coordinates, manhole centred at $x, y = 0, 0$ (mm)
Φ_p	Pipe diameter (mm)
Φ_{lid}	Lid opening diameter (mm)
Φ_m	Manhole diameter (mm)

ORCID

Fabio Muraro  <http://orcid.org/0000-0003-3843-2688>

References

- Abily, M., Bertrand, N., Delestre, O., Gourbesville, P., & Duluc, C. M. (2016). Spatial global sensitivity analysis of high resolution classified topographic data use in 2D urban flood modelling. *Environmental Modelling & Software*, 77, 183–195. <https://doi.org/10.1016/j.envsoft.2015.12.002>
- Addison-Atkinson, W., Chen, A. S., Memon, F. A., & Chang, T. (2022). Modelling urban sewer flooding and quantitative microbial risk assessment: A critical review. *Journal of Flood Risk Management*, 15(4), e12844. <https://doi.org/10.1111/jfr3.12844>
- Andrews, B. J., Cardenas, M. B., & Bennett, P. C. (2011). Analysis of turbulent nonisothermal mixing between a jet and cooler ambient water using thermal imagery. *Geochemistry, Geophysics, Geosystems*, 12(7), Q07022. <https://doi.org/10.1029/2011GC003530>
- Arques, S. R., Rubinato, M., Nichols, A., & Shucksmith, J. D. (2018). Cost effective measuring technique to simultaneously quantify 2D velocity fields and depth-averaged solute concentrations in shallow water flows. *Flow Measurement and Instrumentation*, 64, 213–223.
- Beg, M. N. A., Rubinato, M., Carvalho, R. F., & Shucksmith, J. D. (2020). CFD modelling of the transport of soluble pollutants from sewer networks to surface flows during urban flood events. *Water*, 12(9), 2514. <https://doi.org/10.3390/w12092514>
- Biggs, H., Smart, G., Doyle, M., Eickelberg, N., Aberle, J., Randall, M., & Detert, M. (2023). Surface velocity to depth-averaged velocity—a review of methods to estimate alpha and remaining challenges. *Water*, 15(21), 3711. <https://doi.org/10.3390/w15213711>
- Cardenas, M. B., Neale, C. M. U., Jaworowski, C., & Heasler, H. (2011). High-resolution mapping of river-hydrothermal water mixing: Yellowstone national park. *International Journal of Remote Sensing*, 32(10), 2765–2777. <https://doi.org/10.1080/01431161003743215>
- Carmer, C., Rummel, A., & Jirka, G. (2009). Mass transport in shallow turbulent wake flow by planar concentration analysis technique. *Journal of Hydraulic Engineering*, 135(4), 257–270. [https://doi.org/10.1061/\(ASCE\)0733-9429\(2009\)135:4\(257\)](https://doi.org/10.1061/(ASCE)0733-9429(2009)135:4(257))
- Chen, Y., Shi, X., Jin, X., & Jin, P. (2022). Characteristics of overflow pollution from combined sewer sediment: Formation, contribution and regulation. *Chemosphere*, 298, 134254. <https://doi.org/10.1016/j.chemosphere.2022.134254>
- Dahlke, H. E., Easton, Z. M., Lyon, S. W., Todd Walter, M., Destouni, G., & Steenhuis, T. S. (2012). Dissecting the variable source area concept - subsurface flow pathways and water mixing processes in a hillslope. *Journal of Hydrology*, 420–421, 125–141. <https://doi.org/10.1016/j.jhydrol.2011.11.052>
- Daksiya, V., Mandapaka, P. V., & Lo, E. Y. M. (2021). Effect of climate change and urbanisation on flood protection decision-making. *Journal of Flood Risk Management*, 14:e12681. <https://doi.org/10.1111/jfr3.12681>
- de Almeida, G. A. M., Bates, P., & Ozdemir, H. (2018). Modelling urban floods at submetre resolution: Challenges or opportunities for flood risk management? *Journal of Flood Risk Management*, 11, S855–S865. <https://doi.org/10.1111/jfr3.12276>
- Fagour, C., Proust, S., & Mignot, E. (2022). Water pollution during floods: A protocol for measuring concentration and calculating mass discharge across a straight street. In Ana Maria Ferreira da Silva, Colin Rennie, Susan Gaskin, Jay Lacey, & Bruce MacVicar (Eds.), *River flow 2022* (pp. 920–927). CRC Press.
- Fagour, C., Proust, S., & Mignot, E. (2024). A laboratory experiment on the pollutant transport in a flooded street network. *Journal of Hydrology*, 640, 131603. <https://doi.org/10.1016/j.jhydrol.2024.131603>
- Genouel, M., Comby, E., Le Lay, Y. F., & Biron, P. (2024). Urban flooding and the resultant pollution: What French-speaking scientists make of it? *Anthropocene*, 46, 100436. <https://doi.org/10.1016/j.ancene.2024.100436>
- Ghostine, R., Kesserwani, G., Vazquez, J., Rivière, N., Ghenaïm, A., & Mose, R. (2009). Simulation of supercritical flow in crossroads: Confrontation of a 2D and 3D numerical approaches to experimental results. *Computers & Fluids*, 38(2), 425–432. <https://doi.org/10.1016/j.compfluid.2008.05.003>
- Guymier, I., Dennis, P., O'Brien, R., & Saiyudthong, C. (2005). Diameter and surcharge effects on solute transport across surcharged manholes. *Journal of Hydraulic Engineering. American Society of Civil Engineers*, 131(4), 312–321. [https://doi.org/10.1061/\(ASCE\)0733-9429\(2005\)131:4\(312\)](https://doi.org/10.1061/(ASCE)0733-9429(2005)131:4(312))
- Jimoh, M., & Abolfathi, S. (2022). Modelling pollution transport dynamics and mixing in square manhole overflows. *Journal of Water Process Engineering*, 45, 102491. <https://doi.org/10.1016/j.jwpe.2021.102491>
- Mannina, G., & Viviani, G. (2010). An urban drainage stormwater quality model: Model development and uncertainty quantification. *Journal of Hydrology*, 381(3–4), 248–265. <https://doi.org/10.1016/j.jhydrol.2009.11.047>
- Mark, O., Jørgensen, C., Hammond, M., Khan, D., Tjener, R., Erichsen, A., & Helwig, B. (2018). A new methodology for modelling of health risk from urban flooding exemplified by cholera – case Dhaka, Bangladesh. *Journal of Flood Risk Management*, 11(S1), S28–S42. <https://doi.org/10.1111/jfr3.12182>
- Martins, R., Kesserwani, G., Rubinato, M., Lee, S., Leandro, J., Djordjević, S., & Shucksmith, J. D. (2017). Validation of 2D shock capturing flood models around a surcharging manhole. *Urban Water Journal*, 14(9), 892–899. <https://doi.org/10.1080/1573062X.2017.1279193>
- Martins, R., Rubinato, M., Kesserwani, G., Leandro, J., Djordjević, S., & Shucksmith, J. D. (2018). On the characteristics of velocity fields in the vicinity of manhole inlet grates during flood events. *Water Resources Research*, 54(9), 6408–6422. <https://doi.org/10.1029/2018WR022782>
- Mignot, E., Paquier, A., & Rivière, N. (2008). Experimental and numerical modeling of symmetrical four-branch

- supercritical. *Journal of Hydraulic Research*, 46(6), 723–738.
- Mignot, E., Riviere, N., & Dewals, B. (2023). Formulations and diffusivity coefficients of the 2D depth-averaged advection-diffusion models: A literature review. *Water Resources Research*, 59(12), e2023WR035053. <https://doi.org/10.1029/2023WR035053>
- Mignot, E., Zeng, C., Dominguez, G., Li, C. W., Rivière, N., & Bazin, P. H. (2013). Impact of topographic obstacles on the discharge distribution in open-channel bifurcations. *Journal of Hydrology*, 494, 10–19. <https://doi.org/10.1016/j.jhydrol.2013.04.023>
- Moodi, S., Mahdizadeh, H., Shucksmith, J., Rubinato, M., & Azhdary Moghaddam, M. (2024). Experimental and numerical modelling of water waves in sewer networks during sewer/surface flow interaction using a coupled ODE-SWE solver. *Journal of Flood Risk Management*, 17(1), e12953. <https://doi.org/10.1111/jfr3.12953>
- Muraro, F., Shucksmith, J. D., Addison-Atkinson, W., Fagour, C., Gostiaux, L., Nathalie, G., Nichols, A., Mignot, E., & Rubinato, M. (2025). Experimental characterisation of soluble contaminant transport from surcharging sewer infrastructure within shallow urban floods - Datasets. V2 Zenodo. <https://doi.org/10.5281/zenodo.16936519>
- National Infrastructure Commission. (2022). Reducing the risk of surface water flooding. <https://nic.org.uk/studies-reports/>.
- Pender, G. (2006). Briefing: Introducing the flood risk management research consortium. *Proceedings of the Institution of Civil Engineers - Water Management*, 159(1), 3–8. <https://doi.org/10.1680/wama.2006.159.1.3>
- Riviere, N., Pouchoulin, S., Cai, W., Lipeme Kouyi, G., Le Coz, J., & Mignot, E. (2024). A new pH-based tracing method for flow mixing studies in closed-loop experimental flumes: Evaluation in an open-channel confluence. *Environmental Fluid Mechanics*, 24, 1123–1142. <https://doi.org/10.1007/s10652-024-09990-0>
- Rubinato, M. (2015). *Physical scale modelling of urban flood systems* [PhD thesis]. University of Sheffield. [oai:theses.whiterose.ac.uk:9270](https://oai.theses.whiterose.ac.uk:9270)
- Rubinato, M., Helms, L., Vanderlinden, M., Hart, J., & Martins, R. (2022). Flow exchange, energy losses and pollutant transport in a surcharging manhole linked to street profiles. *Journal of Hydrology*, 604, 127201. <https://doi.org/10.1016/j.jhydrol.2021.127201>
- Rubinato, M., Martins, R., Kesserwani, G., Leandro, J., Djordjević, S., & Shucksmith, J. (2017). Experimental calibration and validation of sewer/surface flow exchange equations in steady and unsteady flow conditions. *Journal of Hydrology*, 552, 421–432. <https://doi.org/10.1016/j.jhydrol.2017.06.024>
- Rutherford, J. C. (1994). *River mixing*. John Wiley.
- Sämann, R., Graf, T., & Neuweiler, I. (2019). Modeling of contaminant transport during an urban pluvial flood event—the importance of surface flow. *Journal of Hydrology*, 568, 301–310. <https://doi.org/10.1016/j.jhydrol.2018.10.002>
- Teng, J., Jakeman, A. J., Vaze, J., Croke, B. F. W., Dutta, D., & Kim, S. (2017). Flood inundation modelling: A review of methods, recent advances and uncertainty analysis. *Environmental Modelling & Software*, 90, 201–216. <https://doi.org/10.1016/j.envsoft.2017.01.006>
- Tscheikner-Gratl, F., Bellos, V., Schellart, A., Moreno-Rodenas, A., Muthusamy, M., Langeveld, J., Clemens, F., Benedetti, L., Angel Rico-Ramirez, M., Fernandes de Carvalho, R., Breuer, L., Shucksmith, J., Heuvelink, G. B. M., & Tait, T. (2019). Recent insights on uncertainties present in integrated catchment water quality modelling. *Water Research*, 150, 368–379. <https://doi.org/10.1016/j.watres.2018.11.079>